SolarPACES 2022, 28th International Conference on Concentrating Solar Power and Chemical Energy Systems
Thermal Energy Storage Materials, Media, and Systems
https://doi.org/10.52825/SolarPACES.v1i.614

Published: 28 Mar. 2024

Dynamic Corrosion of Carbonate Salt for 3rd Generation CSP Plants

Luis González-Fernández[1][https://orcid.org/0000-0003-1800-3712], Mikel Intxaurtieta-Carcedo[1][https://orcid.org/0000-0003-2163-8444], Oleksandr Bondarchuk[2][https://orcid.org/0000-0001-7380-8930], and Yaroslav Grosu[1,3][https://orcid.org/0000-0001-6523-1780]

[1] Centre for Cooperative Research on Alternative Energies (CIC energiGUNE), Basque Research and Technology Alliance (BRTA), Spain

[2] International Iberian Nanotechnology Laboratory, Portugal

[3] Institute of Chemistry, University of Silesia in Katowice, Poland

Abstract. Eutectic ternary carbonate salt is one of the candidates for 3rd generation concentrated solar power (CSP) plants. Gen3 CSP targets higher operation temperatures, which strengthens the corrosivity issues associated to molten salts. Although there are corrosion studies for this carbonate salt in static conditions, the effect of salt flow is not fully understood. In this work, corrosion experiments under static and dynamic conditions are compared for SS310 subjected to ternary carbonate salt at 600ºC.

The corrosion layer formed during static and dynamic tests were completely characterized by means of SEM-EDX and XRD (surface and cross-section). The corrosion products deposited in the salt during the experiment were analyzed by ICP-OES.

The tests performed under dynamic conditions demonstrated an increase spallation of the corrosion layer. This spallation produced a thinner scale and exposed the Cr containing phase to the molten salt, fostering its dissolution. These results confirmed the significant effect of dynamic conditions on the corrosivity of eutectic ternary carbonate salt and the importance of assessing them in the design of 3rd generation CSP plants.

Keywords: Corrosion Under Dynamic Conditions, Third Generation Concentrated Solar Power, Thermal Energy Storage (TES), Molten Salts, High-Temperature, Eutectic Ternary Carbonate Salt: Li_2CO_3-Na_2CO_3-K_2CO_3

1. Introduction

In a global situation of growing energy demand and requirement of lowering greenhouse gases, renewable energies must be fostered. Among them, concentrated solar power (CSP) is the only one with mature storage solution at industrial scale: molten salt-based thermal energy storage (TES) systems [1]. The feasibility of implementing a storage unit makes CSP dispatchable and lowers its LCOE [2].

Current industrial TES systems employ the two-tank technology and solar salt ($NaNO_3$-KNO_3, 60%-40% in wt%) as thermal storage media [1]. The use of solar salts limits the operational temperature range below 565 ºC, also limiting the overall efficiency of the CSP plant. A working temperature rise would increase the efficiency and rentability of next generation plants [3]. Carbonate and chloride salt mixtures have been proposed to achieve this target. Chloride salts, although being the most cost-effective option, present higher corrosivity [4]

and require elaborated processes to prepare the blends [5,6]. Carbonate mixtures are less attractive in price terms, but present lower corrosion issues, their preparation is much simpler and show enhanced thermophysical properties [1,7]. The eutectic ternary carbonate salt (34.5% K_2CO_3 - 33.4% Na_2CO_3 - 32.1% Li_2CO_3, wt%) is one of the most promising candidates among these mixtures.

In this sense, the corrosivity of carbonate salts in static conditions has been extensively analyzed in literature, and concretely numerous works reported results for the eutectic ternary system [8-13]. However, to the best of our knowledge, just one paper addressing the corrosion of K_2CO_3-Na_2CO_3-Li_2CO_3 in dynamic configuration has been published [14]. The authors reported large metal loss for coated and uncoated P91 alloy at 650 ºC, but surprisingly higher spallation was found in static conditions.

Therefore, there is a lack of studies with the salt under dynamic conditions, which is closer to real application. In this work, we investigate the modifications of the corrosion process due to the salt pumping for ternary eutectic carbonate mixture and 310 stainless steel at 600 ºC.

2. Materials and Techniques

Eutectic ternary carbonate salt was employed for the corrosion tests: 34.5% K_2CO_3 - 33.4% Na_2CO_3 - 32.1% Li_2CO_3 (weight concentration). The components of the carbonate salt were purchased from Sigma-Aldrich (purity > 99%). The tree carbonates were dried in oven for 12 hours at 120 ºC before mixing. The samples and rotation-transmitting rods employed in this work were made of SS310, whose composition is detailed in Table 1.

Table 1. Chemical composition of SS310 (wt%).

	Fe	Ni	Cr	Mn	Si	P	C	S
SS310	Balance	19.1	24.9	1.81	0.64	0.03	0.05	0.01

The experimental setup developed for conducting the experiments is shown in Figure 1. The electric motor above the furnace produces a rotation that is transmitted by the rod to the cross-shaped sample attached to the bottom end, located inside the crucible containing the salt. The junction between the engine and the rod is electrically insulated. This configuration reproduces the dynamic corrosion conditions in the inner walls of pipes due to salt pumping.

Cross-shaped SS310 samples were employed, for producing 4 pieces to be studied after the test. A total of 685 g of carbonate salt were used to ensure the complete immersion of the sample during the experiment. For running the experiment, the temperature was raised to 450 ºC at 5 ºC/min; then, 1 hour at isothermal conditions to ensure complete melting of the salt; followed by a heating to 650 ºC with the previous rate. When the desired temperature was reached, the rotation was started, and the temperature maintained for 600 hours. The test was carried out at a spinning rate of 60 rpm, which means a linear velocity in the central part of the petals of the sample of $\sim$ 0.2 m/s.

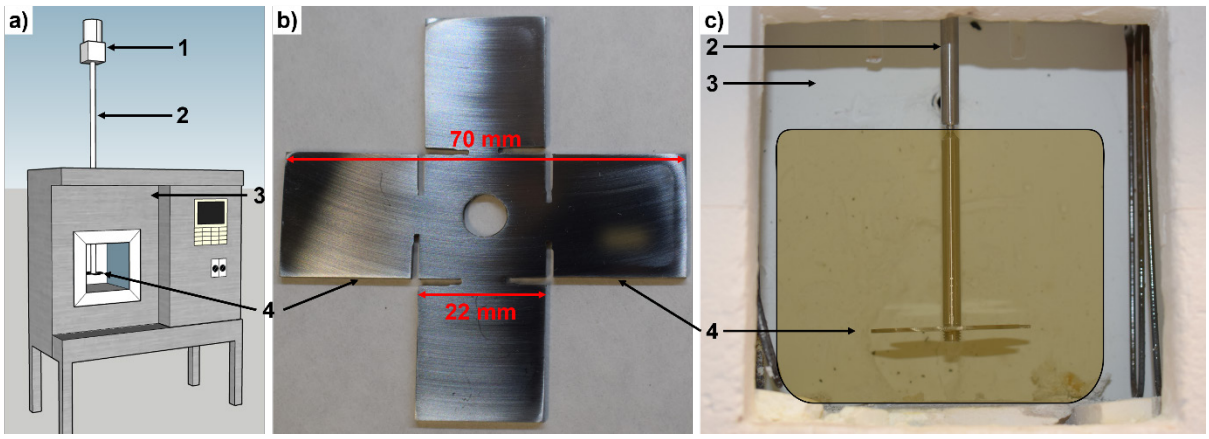

Figure 1. Experimental setup for dynamic corrosion tests: schematic view (a) and photos (b, c) of electric motor (1), rotation-transmitting rod (2), furnace (3) and SS310 sample (4).

After the dynamic experiment, another corrosion test was performed without rotating the sample but with the same experimental configuration. The results in static conditions were used as reference to determine the effect of salt movement on the corrosion process.

The samples were characterized after the corrosion tests by scanning electron microscope (SEM) –Quanta 200 FEG equipped with energy-dispersive X-ray spectroscopy (EDX)– and X-ray diffraction (XRD) –Bruker D8 Discover diffractometer equipped with a LINXEYE detector using CuKα1 radiation (λ = 1.5418 Å) in Bragg-Brentano θ:2θ geometry–. The carbonate salt was examined by inductively coupled plasma optical emission spectroscopy (ICP-OES) –Horiba Ultima 2 model in conjunction with a AS500 autosampler and Activanalyst software–.

3. Results and Discussion

The first visual analysis of the samples after the corrosion tests showed a significant spallation of the corrosion layer in both conditions. However, the sample tested in static conditions presented lower spallation extend, since there were still corrosion scales loosely attached to the samples. These scales were not observed for the dynamic case because the rotation forced their complete detachment.

The difference between the samples tested in dynamic and static cases was confirmed by SEM analysis (Fig. 2). The beginning of the corrosion layer spallation is appreciated in Fig. 2b. Traces of these spallations are still present in the regions where the layer is already separated. However, the samples tested in static conditions present totally different surface features (Fig. 2a), with three stacked layers observed. The oxide crystals located in top and bottom layers are significantly bigger than the ones in middle layer, which produce a smoother surface. In the bottom layer though, protuberances are appreciated. High magnification images (Fig. 2 c & d) were acquired in the corrosion layer region closer to the metallic matrix, below detached scale. The sample tested in static conditions presents big octahedral formation (Fig. 2c), while dynamic conditions lead to smaller crystals (Fig. 2d). This difference is due to the salt flow in dynamic conditions, which avoids the big crystals growth, contrary to static conditions, which enhance bigger oxide crystals formation.

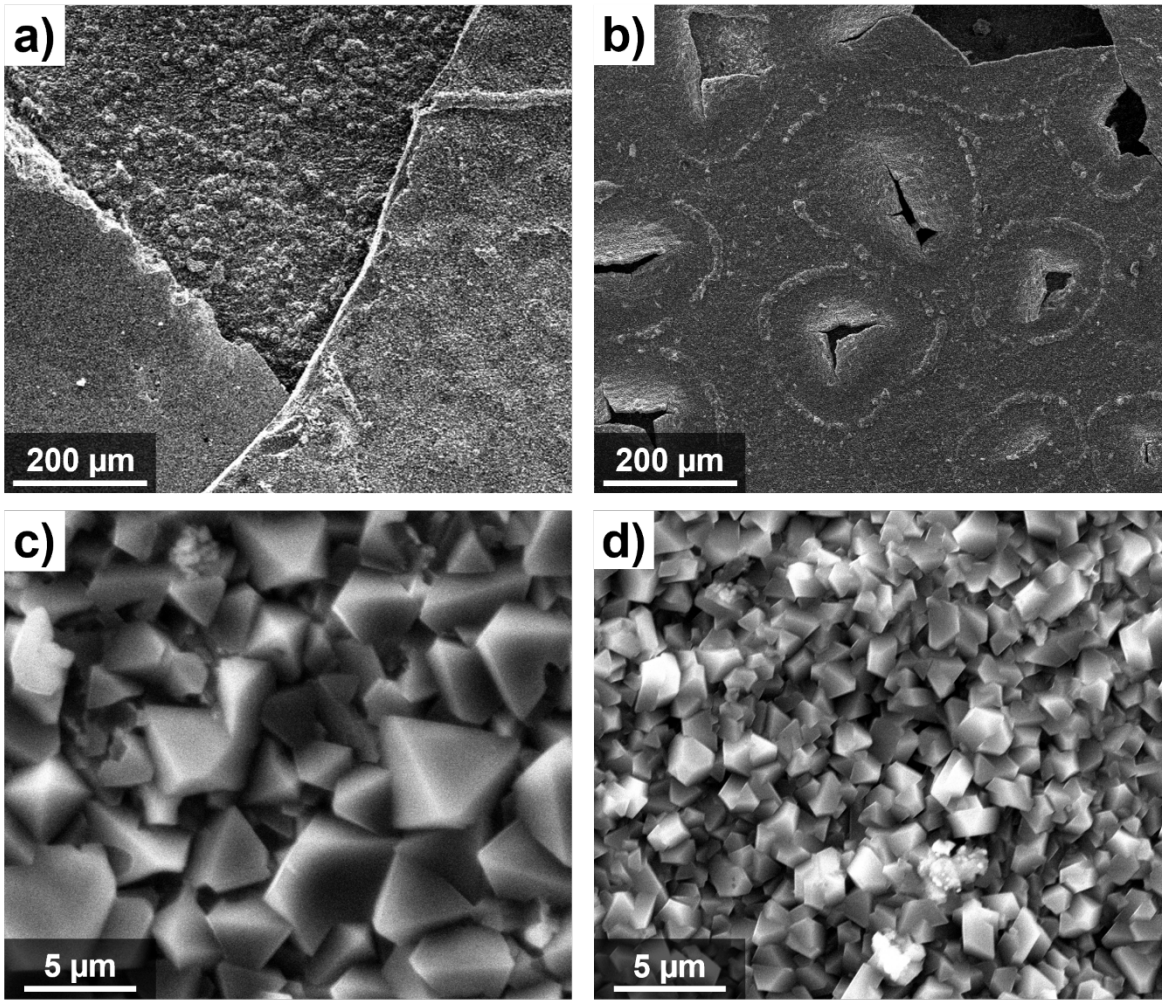

Figure 2. SEM images of the SS310 samples after 600 hours corrosion experiment at 600 °C under static (a and c) and dynamic (b and d) conditions.

As it is shown in Fig. 3, the thickness of the corrosion layer produced under dynamic and static conditions is remarkably different. Since the rest of experimental parameters (temperature, duration, setup) were the same in both cases, this difference is only attributable to the rotation of the SS310 sample. When the corrosion layer reaches certain thickness, the salt flow produces the spallation of the outer region, which is loosely attached. However, in static conditions the detachment is not forced and, consequently, the resulting layer is thicker.

For the samples tested in dynamic conditions, the spallation extent prevented from obtaining of an average corrosion rate. On the other hand, for static conditions, the determined average corrosion rate was 466 ± 3 µm/year, with a variability ranging from 364 to 668 µm/year. This average value is within the limits of previously reported data, between 73 and 438 µm/year, but it is significantly larger than the reported average corrosion rate, 157.0 ± 41.5 µm/year [11,12]. Nevertheless, the deviation obtained in this work is significantly lower. These two features indicate lower spallation in this work, giving rise to thicker and more homogeneous corrosion layer. These differences could be explained by different salt mass-to-stainless steel superficial area ratio. The present study tested samples with approximately 7000 mm^2 of external surface in 685 g of carbonate salt, while in refs [11,12], 5 g of salt were employed for samples with 1000 mm^2 superficial area. Thus, 20 times higher salt to metal ratio was used in this work.

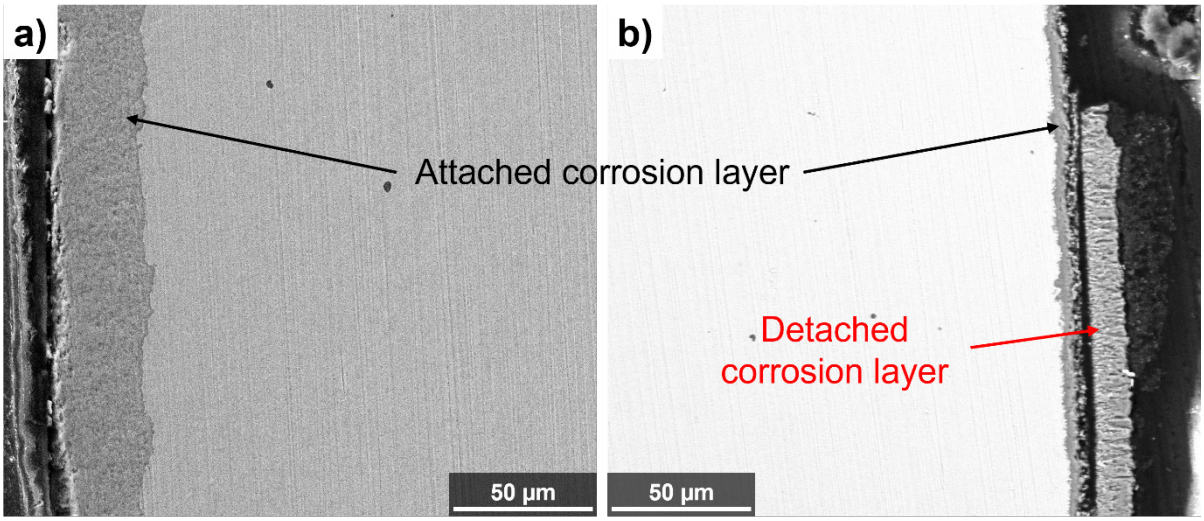

Figure 3. SEM images of the cross-section of the SS310 samples after 600 hours corrosion experiment at 600 °C for a) static and b) dynamic test.

In Fig. 4, the diffractograms of dynamically and statically tested samples are plotted, together with pristine SS310 as reference. There are two XRD patterns corresponding to the static case, one representing the tested piece and the other the loosely attached scale, that was removed and analyzed independently.

It can be observed that the corrosion layer formed in dynamic conditions is composed of $LiCrO_2$ and $Li_{1.05}(Fe/Ni)_{0.95}O_2$. As well, since the corrosion layer is thin enough, the Fe/Ni/Cr peaks, corresponding to the SS310 substrate, are also present in the pattern.

For static samples, the contribution from the substrate is not appreciated, in agreement with the thicker layer. Moreover, some additional oxides are included into the corrosion layer: $Li(Fe/Ni)_5O_8$ and $MnNi_6O_8$, iron oxide (Fe_2O_3) and small contribution of K_2NiO_2. Therefore, in static case the presence of iron oxides is higher than in dynamic conditions. This points to reduced adhesion of Fe and Ni oxides, and their consequently removal in dynamic conditions. This fact agrees with the composition of the removed scale, the same of layer attached to the piece except $LiCrO_2$.

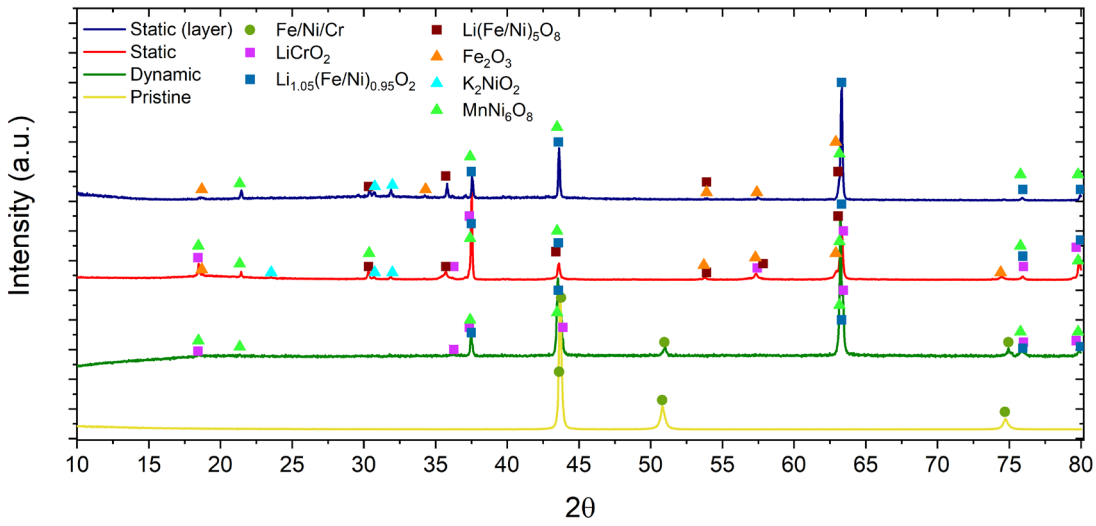

Figure 4. XRD patterns of samples after 600 hours corrosion experiment at 600 °C for static (piece and removed layer) and dynamic test (piece). Pristine SS310 is included as reference.

The location of the phases in the corrosion layer can be determined by combining the XRD results with the SEM-EDX mapping of the cross-section of samples. It can be appreciated that in the sample tested in dynamic conditions (Fig. 5b), the presence of Cr is limited to the region closer to the substrate. Hence, the $LiCrO_2$ is just located below the $Li_{1.05}(Fe/Ni)_{0.95}O_2$ phase. This stratification feature of the corrosion layer was previously described for ternary carbonate salt in static tests for SS310 [12] and SS316L [13].

Considering the EDX results obtained for the static sample, there are three different regions in the corrosion layer in terms of composition, as it is represented in Fig. 5a. It is remarkable that in this case the Cr is present throughout the corrosion layer, especially in the outer region, where the Ni concentration is lower. Thus, it can be stated that the Cr diffuses from the SS310 to the corrosion layer. The same behavior should be expected for the sample subjected to dynamic conditions but, however, the Cr containing phase was just found in the inner part of the corrosion layer (Fig. 5b), due to the Cr dissolution into the salt. The outer scale with high Fe content can be assigned to the Fe_2O_3 phase. An external layer of Fe oxides was also reported in ref. [13].

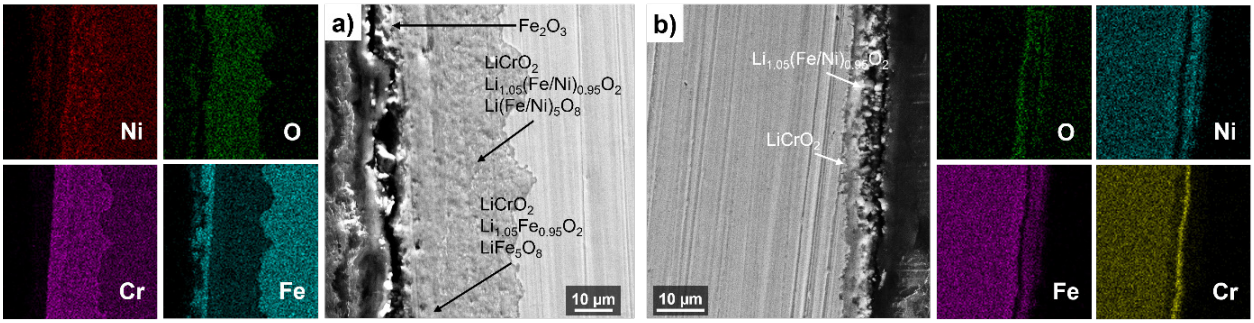

Figure 5. SEM images and EDX mapping of the cross-section of the SS310 samples after 600 hours corrosion experiment at 600 ºC under a) static and b) dynamic conditions.

The dissolution of Cr into the salt is promoted under dynamic conditions. Firstly, because the rotation produces a continuous spallation process, which removes the Fe/Ni oxides and exposes the $LiCrO_2$ phase to the salt. Secondly, because the salt flow ensures that the $LiCrO_2$ is in contact with fresh salt, which increases Cr concentration gradient and encourages its dissolution. On the contrary, in static conditions, the renovation of salt in contact with the corrosion layer is slower, reducing the dissolution extent.

To confirm the different dissolution extent in static and dynamic conditions, the salts after conducting the experiments were analyzed by ICP-OES. The results are detailed in Table 2. As expected, the Cr content in the salt of the dynamic experiment is more than twofold the one of the static case. This magnitude of dissolution under dynamic conditions compared to static case, together with the increased spallation, suggest that the corrosion rate for dynamic configuration is, at least, twice higher. Finally, Mg is a common impurity in molten salts, and Mn is a component of the SS310. Their content is equivalent in both cases taking into account the experimental uncertainty.

Table 2. Concentration of impurities in the salts after corrosion tests determined by ICP-OES.

	Cr (ppm)	Mg (ppm)	Mn (ppm)
Dynamic test	1.560	0.752	0.080
Static test	0.617	0.712	0.103

An extension of this work with further analyses has been published in ref [15].

4. Conclusions

In this work, the impact of the dynamic conditions on the corrosion was studied for SS310 in the eutectic K_2CO_3-Na_2CO_3-Li_2CO_3 salt at 600 ºC under air atmosphere. The flow of the molten salt was replicated by rotating an immersed sample, to mimic the real working conditions. A static test was employed as reference. The following conclusions can be highlighted:

1. The corrosion of SS310 in molten ternary carbonate salt was significantly increased by dynamic conditions compared to the static case. The spallation of the corrosion layer was drastically extended in dynamic experiment, which gave rise to a thinner and less protective layer.
2. The increase of Cr dissolution into the molten salt for dynamic conditions was confirmed by ICP analysis. More than twofold concentration of Cr was found for dynamic test.
4. XRD and SEM-EDX analysis were employed to identify the phases formed during the corrosion process and their location the corrosion layer.
5. The steel-to-molten salt ratio can influence the obtained absolute values of the corrosion rates.

This work highlights the significant effect of dynamic conditions on the corrosion process of ternary eutectic carbonate salt. The major consequences are the increased spallation and the Cr dissolution under dynamic conditions compared to static experiment. Considering these effects, the standard static immersion corrosion tests are not sufficient for evaluating the resistance of components in contact with pumped salt. Experiments under dynamic conditions are necessary for designing 3rd generation CSP plants.

Data availability statement

Data will be made available on request.

Author contributions

Luis González-Fernández: Conceptualization, Methodology, Formal analysis, Investigation, Writing-Original draft preparation, Writing- Review and Editing, Supervision. Mikel Intxaurtieta-Carcedo: Resources. Oleksandr Bondarchuk: Formal analysis, Investigation, Writing-Review and Editing. Yaroslav Grosu: Conceptualization, Methodology, Formal analysis, Writing- Review and Editing, Supervision, Project administration.

Competing interests

The authors declare no competing interests.

Acknowledgement

The authors express their sincere thanks to Cristina Luengo and Yagmur Polat for their technical support, and to Diana Lopez for her assistance with ICP measurements.

References

1. Angel G. Fernández, Judith Gomez-Vidal, Eduard Oró, Alan Kruizenga, Aran Solé, Luisa F. Cabeza, “Mainstreaming commercial CSP systems: A technology review,” Renew. Energy, 140, 152-176, 2019, https://doi.org/10.1016/j.renene.2019.03.049
2. J. Lilliestam, T. Barradi, N. Caldés, M. Gomez, S. Hanger, J. Kern, N. Komendantova, M. Mehos, W.M. Hong, Z. Wang, A. Patt, “Policies to keep and expand the option of concentrating solar power for dispatchable renewable electricity,” Energy Pol., 116, 193–197, 2018, https://doi.org/10.1016/j.enpol.2018.02.014
3. M. Mehos, C. Turchi, J. Vidal, M. Wagner, Z. Ma, C. Ho, W. Kolb, C. Andraka, A. Kruizenga, “Concentrating solar power Gen3 demonstration roadmap,” in: National Renewable Energy Lab. (NREL), Golden, CO (United States), 2017.
4. W. Ding, A. Bonk, T. Bauer, “Corrosion behavior of metallic alloys in molten chloride salts for thermal energy storage in concentrated solar power plants: A review,” Front. Chem. Sci. Eng., 12, 564–576, 2018, https://doi.org/10.1007/s11705-018-1720-0
5. J.C. Vidal, N. Klammer, “Molten chloride technology pathway to meet the U.S. DOE sunshot initiative with Gen3 CSP,” AIP Conf. Proc., 2126, 080006, 2019, https://doi.org/10.1063/1.5117601
6. W. Ding, J. Gomez-Vidal, A. Bonk, T. Bauer, “Molten chloride salts for next generation CSP plants: Electrolytical salt purification for reducing corrosive impurity level,” Sol. Energy Mater. Sol. Cells, 199, 8–15, 2019, https://doi.org/10.1016/j.solmat.2019.04.021
7. R. Raud, R. Jacob, F. Bruno, G. Will, T.A. Steinberg, “A critical review of eutectic salt property prediction for latent heat energy storage systems,” Renew. Sustain. Energy Rev., 70, 936–944, 2017, https://doi.org/10.1016/j.rser.2016.11.274
8. A.G. Fernández, F. Pineda, M. Walczak, L.F. Cabeza, “Corrosion evaluation of alumina-forming alloys in carbonate molten salt for CSP plants,” Renew. Energy, 140, 227–233, 2019, https://doi.org/10.1016/j.renene.2019.03.087
9. M. Sarvghad, O. Muransky, T.A. Steinberg, J. Hester, M.R. Hill, G. Will, “On the effect of cold-rolling on the corrosion of SS316L alloy in a molten carbonate salt,” Sol. Energy Mater. Sol. Cell, 202, 110136, 2019, https://doi.org/10.1016/j.solmat.2019.110136
10. S.P. Sah, “Corrosion of 304 stainless steel in carbonates melt– a state of enhanced dissolution of corrosion products,” Corrosion Science, 169, 108535, 2020, https://doi.org/10.1016/j.corsci.2020.108535
11. Y. Grosu, A. Anagnostopoulos, B. Balakin, J. Krupanek, M.E. Navarro, L. González-Fernández, Y. Ding, A. Faik, “Nanofluids based on molten carbonate salts for high-temperature thermal energy storage: Thermophysical properties, stability, compatibility and life cycle analysis,” Sol. Energy Mater. Sol. Cells, 220 110838, 2021, https://doi.org/10.1016/j.solmat.2020.110838J.
12. Y. Grosu, A. Anagnostopoulos, M.E. Navarro, Y.Ding, A. Faik, “Inhibiting hot corrosion of molten Li2CO3-Na2CO3-K2CO3 salt through graphitization of construction materials for concentrated solar power,” Sol. Energy Mater. Sol. Cells, 215, 110650, 2020, https://doi.org/10.1016/j.solmat.2020.110650
13. J. Luo, C.K. Deng, N.H. Tariq, N. Li, R.F. Han, H.H. Liu, J.Q. Wang, X.Y. Cui, T.Y. Xiong, “Corrosion behavior of SS316L in ternary Li2CO3–Na2CO3–K2CO3 eutectic mixture salt for concentrated solar power plants,” Sol. Energy Mater. Sol. Cells, 217, 110679, 2020, https://doi.org/10.1016/j.solmat.2020.110679
14. P. Audigié, V. Encinas-Sánchez, S. Rodríguez, F.J. Pérez, A. Agüero, “High temperature corrosion beneath carbonate melts of aluminide coatings for CSP application,” Sol. Energy Mater. Sol. Cells, 210, 110514, 2020, https://doi.org/10.1016/j.solmat.2020.110514
15. L. González-Fernández, M. Intxaurtieta-Carcedo, O. Bondarchuk, Y. Grosu, “Effect of dynamic conditions on high-temperature corrosion of ternary carbonate salt for thermal energy storage applications”, Sol. Energy Mater. Sol. Cells, 240, 111666, 2022, https://doi.org/10.1016/j.solmat.2022.111666